

Crystal growth and properties of the disordered crystal Yb:SrLaAlO₄: A promising candidate for high-power ultrashort pulse lasers

Received 00th January 20xx,
Accepted 00th January 20xx

DOI: 10.1039/x0xx00000x

www.rsc.org/

Zhongben Pan,^{ab} Xiaojun Dai,^a Yuanhua Lei,^a Huaqiang Cai,^a Josep Maria Serres,^c Magdalena Aguiló,^c Francesc Díaz,^c Jie Ma,^d Dingyuan Tang,^d Elena Vilejshikova,^e Uwe Griebner,^b Valentin Petrov,^b Pavel Loiko^f and Xavier Mateos^{*c}

A high quality Yb³⁺-doped strontium lanthanum aluminate crystal, Yb:SrLaAlO₄ (Yb:SLA) is grown by the Czochralski method. It is tetragonal (sp. gr. *I4/mmm*, $a = b = 3.7536 \text{ \AA}$, $c = 12.6253 \text{ \AA}$). Room- and low-temperature spectroscopy of Yb³⁺ ions in this crystal are studied. The Stark splitting is resolved. Absorption, stimulated-emission (SE) and gain cross-sections are determined with polarized light. In the spectral range of laser emission, the maximum σ_{SE} is $0.57 \times 10^{-20} \text{ cm}^2$ at 1047 nm for σ polarization. The polarized Raman spectra of Yb:SLA are presented. Thermal properties of Yb:SLA are characterized in terms of the linear thermal expansion, specific heat and thermal conductivity. The latter is as high as 6.06 and 4.30 $\text{Wm}^{-1}\text{K}^{-1}$ along the *a*- and *c*-axes, respectively (at room temperature). Broadband tuning of a continuous-wave (CW) Yb:SLA laser, from 1011 to 1082 nm has been achieved. Due to its good thermal properties, broad and smooth gain spectra, Yb:SLA is a promising material for power-scalable, broadly tunable CW and sub-100 fs mode-locked lasers at $\sim 1 \mu\text{m}$.

Introduction

In recent decades, diode-pumped solid-state lasers (DPSSLs) have found multiple applications in research and industry. In the mode-locked (ML) operation mode, such lasers are capable of generating femtosecond (fs) pulses. Due to the high quantum efficiency and broadband emission characteristics, ytterbium (Yb³⁺) doped materials were recognized to be almost ideal gain media for fs DPSSLs at $\sim 1 \mu\text{m}$ [1,2].

Among the gain media, rare-earth (RE) doped disordered crystals are suitable for pulse shortening in ML lasers. In such crystals, different passive (host-forming) cations and laser-active RE³⁺ ions (substituting for the passive ions) can randomly occupy the same site or they can be distributed over several types of sites. This leads to a variation of the coordination sphere around the RE³⁺ ions, resulting in a considerable inhomogeneous spectrum line broadening [3,4]. Such a broadening helps for the generation of ultrashort

pulses. Desirably, the disordered crystals should have good thermal, thermo-optic and thermo-mechanical properties to support power scaling and generation of a high-peak power pulsed output.

So far, many Yb³⁺-doped disordered crystals, e.g., Yb:Ca₄YO(BO₃)₃, Yb:NaY(WO₄)₂, Yb:CaLnAlO₄ (Ln = Y or Gd) and Yb,Na:Ca₃(NbGa)_{2-x}Ga₃O₁₂, have been employed for the generation of sub-50 fs pulses at the 1 μm spectral range [5-9]. Pulses as short as 32 fs were generated with Yb³⁺-doped calcium gadolinium aluminate, Yb:CaGdAlO₄ [9], a disordered crystal that belongs to the ABCO₄-type compounds, where A = Ca or Sr, B = Y, La, Nd or Sm, and C = Al or Ga.

Strontium lanthanum aluminate, SrLaAlO₄ (shortly SLA) is another member of the ABCO₄-type compounds. It belongs to the tetragonal system with K₂NiF₄ structure, space group *I4/mmm*. Similarly to the disordered structure of the CaLnAlO₄ crystals, the lattice disorder of SLA results from a random distribution of La³⁺ and Sr²⁺ cations over a single type of site located between two-dimensional layers of corner-connected AlO₆ octahedra. When doped with laser-active RE ions such as Nd³⁺, Yb³⁺ or Tm³⁺, the disordered feature generates a variation of the local crystal field around the active ions resulting in a considerable inhomogeneous spectrum line broadening. Thus, almost flat and broad emission bands are expected, which are suitable for the generation of ultrashort pulses.

Up to now, the characterization of Nd:SLA, including the crystal growth, thermal properties, polarized spectra and laser performance was reported. Pulses as short as 458 fs were

^a Institute of Chemical Materials, China Academy of Engineering Physics, Mianyang, 621900, China

^b Max-Born-Institute for Nonlinear Optics and Short Pulse Spectroscopy, Max-Born-Str. 2a, D-12489 Berlin, Germany

^c Universitat Rovira i Virgili, Departament Química Física i Inorgànica, Física i Cristal·lografia de Materials i Nanomaterials (FICMA-FICNA)-EMaS, Campus Sescelades, E-43007, Tarragona, Spain. E-mail: xavier.mateos@urv.cat

^d School of Electrical and Electronic Engineering, Nanyang Technological University, Singapore 639798, Singapore

^e Center for Optical Materials and Technologies (COMT), Belarusian National Technical University, 65/17 Nezavisimosti Ave., Minsk 220013, Belarus

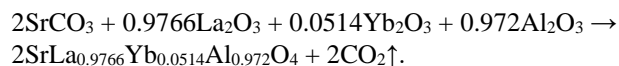
^f ITMO University, 49 Kronverkskiy Pr., 197101 Saint-Petersburg, Russia

achieved from a ML Nd:SLA laser at a central wavelength of 1077.9 nm [10,11]. However, there are no reports about the Yb³⁺-doped SLA crystal. We believe that this is due to the difficulty in obtaining the Yb:SLA crystals of suitable size and good optical quality. Although it was firstly obtained by Brown *et al.* in 1990 and investigated for many years since then, high optical quality, crack and defect-free SLA crystal boules couldn't be easily obtained because of the natural cleavage along the (001) plane, unstable growth process and the existence of a second order transition at 500 K [12-15]. As a consequence, the crystal growth of high quality Yb:SLA is challenging to evaluate its tunable and mode-locked (ML) laser performance.

In this work, the Yb³⁺-doped SLA crystal was successfully grown by the Czochralski (Cz) method. Its structure, anisotropic thermal properties and polarized spectroscopic properties were characterized for the first time. Additionally, the tunable laser operation of Yb:SLA was also investigated as a preliminary step to demonstrate ML performance.

Crystal growth

A 5 at.% Yb³⁺-doped (in the melt) SLA single crystal was grown by the Cz method using an Ar atmosphere in an Ir crucible. The starting materials, SrCO₃ (purity: 4N), La₂O₃ (4N), Al₂O₃ (4N) and Yb₂O₃ (5N), were weighed according to a nearly stoichiometric composition, SrLa_{1.03}Al_{0.97}O₄, with 5 at.% Yb³⁺, and the chemical reaction was as follows:



Then they were mixed, ground and heated at 1473 K for 12 h in a Pt crucible. After the crucible was cooled down to room temperature (RT: 293 K), the mixture was pressed into pellets and again reheated at 1573 K for 12 h.

The synthesized polycrystalline material was placed in an Ir crucible and melted by an intermediate-frequency heater. Usually, to remove the bubbles from the melt and to avoid the formation of polycrystals during the growth process, a temperature of 30–50 K above the melting point is required. The temperature was held at that point for about 2–3 h, and then decreased to the melting point. Additionally, good quality of the crystal might be influenced by the effect of constitutional supercooling, thus some effective measures should be employed, such as lowering the pulling rate to avoid distortions, or increasing the temperature gradient in the melt for a better homogenization. In our experiment, the pulling rate varied from 0.5 to 0.8 mm/h and the crystal rotation speed was kept at 8 to 15 revolutions per minute (rpm). After the growth was completed, the crystal was cooled down to RT at a stepped rate of 15 to 25 K/h.

First, a small crystal was grown on an Ir wire. Then, a seed oriented along the crystallographic *c*-axis was cut from it. However, due to (i) the natural cleavage along the (001)

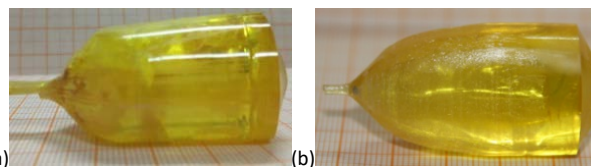


Fig. 1 As-grown Yb:SLA crystal boules, the seed was oriented (a) along the *c*-axis and (b) along the *a*-axis.

plane, (ii) the temperature gradient during the crystal growth and (iii) the anisotropy of thermal expansion (see below), the obtained crystal contained multiple cracks, see Fig. 1a. Thus, a seed oriented along the *a*-axis was chosen for the further crystal growth. An Yb:SLA crystal of large size and good optical quality was finally grown, see Fig. 1b. To obtain a crack-free crystal boule, the temperature gradient and cooling rate (slower and stepped cooling rate) during and after the crystal growth should be optimized.

No scattering centers can be observed under a 5 mW He-Ne laser probe indicating good optical quality. Additionally, the as-grown Yb:SLA crystal shows a yellow color, which is dependent on the temperature gradient at the crystal-melt interface, the melt composition and the oxygen pressure [13]. A similar yellow coloration is typically observed for the Yb:CaGdAlO₄ crystal [16]. It can affect the laser performance in the high-power regime. To eliminate the coloration, the as-grown crystals can be annealed under nitrogen atmosphere mixed with 5% hydrogen [17].

Note that the crystal growth of Yb:SLA is in general similar to that of Yb:CaGdAlO₄. For the former crystal, the growth of high-quality boules is complicated by the natural cleavage along the (001) plane, unstable growth process and the existence of a second order transition at ~500 K. Only after optimizing the growth conditions, including the composition (SrLa_{1.03}Al_{0.97}O₄), temperature gradient, oriented seed, smaller and stepped cooling rate, large size and good optical quality Yb:SLA crystal can be obtained.

By using X-ray fluorescence, the segregation coefficient of Yb³⁺ ions (K_{Yb}) was determined to be 0.235, corresponding to an Yb³⁺ concentration in the Yb:SLA crystal of 1.175 at.%. The relatively low segregation coefficient indicated that the Yb³⁺ ions cannot be easily embedded into the SLA structure. In the SLA lattice, the La³⁺ and Sr²⁺ ions statistically occupy the same site in which they are IX-fold O²⁻ coordinated. The Yb³⁺ ions replace the La³⁺ ones. The low value of K_{Yb} is due to the large mismatch in the ionic radii of La³⁺ and Yb³⁺ (1.216 Å and 1.042 Å, respectively).

Crystal structure

X-ray powder diffraction (XRD) was used to determine the lattice parameters and phase purity of the as-grown Yb:SLA crystal at RT. The results are shown in Fig. 2. A Bruker D8 ADVANCE diffractometer and the Cu K_α line (1.5406 Å) were used. The as-grown crystal consists of a single phase Yb:SLA belonging to the space group D¹⁷_{4h} - *I4/mmm* (No.

139). The structure of Yb:SLA was refined with the Rietveld method, see Fig. 2. The R -factors were $R_{wp} = 13.06\%$, $R_{exp} = 12.94\%$ and the reduced chi-squared value χ^2 was 1.019.

The tetragonal unit cell parameters are $a = b = 3.7562(1)$ Å, $c = 12.6351(2)$ Å, the volume of the unit-cell $V = 178.27(1)$ Å³ and the number of structural units $Z = 2$. The calculated crystal density ρ_{calc} was 5.7490 g/cm³. These results are in close agreement with the data given in the JCPDS card No. 81-0744 for an undoped SLA ($a = 3.7564$ Å, $c = 12.6357$ Å). By using the calculated cell parameters, the Yb³⁺ ion concentration N_{Yb} was determined to be 1.36×10^{20} cm⁻³.

The fractional atomic coordinates and the selected interatomic distances for the Yb:SLA crystal determined with the Rietveld refinement are listed in Table 1 and Table 2, respectively.

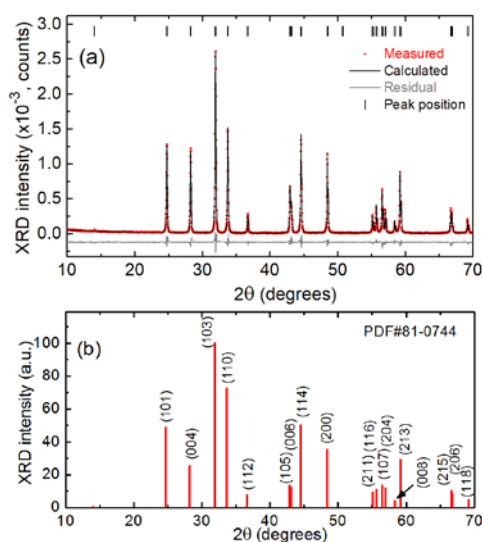


Fig. 2 XRD patterns of the as-grown Yb:SLA crystal measured at RT (a) and standard data (JCPDS card No. 81-0744) (b). Numbers in (b) denote the Miller's indices, (hkl) .

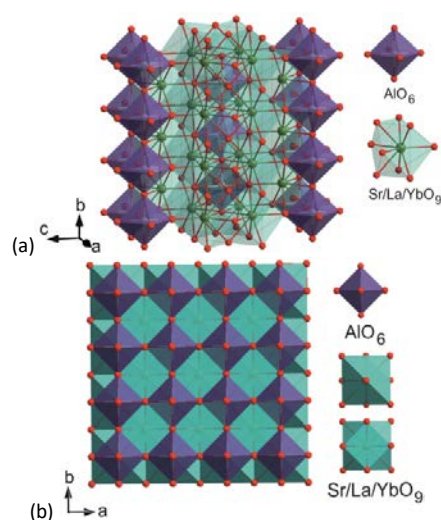


Fig. 3 Structure of the Yb:SLA crystal. Projection to the b - c plane (a) and a - b plane (b).

Table 1. Fractional atomic coordinates for the Yb:SrLaAlO₄ crystal.

Atom	Wyckoff	Site symmetry	x/a	y/b	z/c
Sr	4e	C _{4v}	0	0	0.35849(9)
La	4e	C _{4v}	0	0	0.35849(9)
Yb	4e	C _{4v}	0	0	0.35849(9)
Al	2a	D _{4h}	0	0	0
O1	4c	D _{2h}	0	1/2	0
O2	4e	C _{4v}	0	0	0.17038(8)

Table 2. Selected interatomic distances for the Yb:SrLaAlO₄ crystal.

Polyhedron	Distance	Count	Distance, Å
MO ₉ , M = Sr La Yb	M – O2	×1	2.3768(3)
	M – O1	×4	2.5931(8)
	M – O2	×4	2.6810(1)
	M – M	×1	3.5760(2)
	M – M	×4	3.7562(1)
AlO ₆	M – M	×4	3.8171(1)
	Al – O1	×4	1.8781(1)
	Al – O2	×2	2.1528(1)
	Al – Al	×4	3.7562(1)

The structure of Yb:SLA is illustrated in Fig. 3. In this crystal, the Al³⁺ cations occupy the 2a sites with VI-fold O²⁻ coordination (4×O1 and 2×O2) forming the [AlO₆] octahedra. The Al – O interatomic distances range from 1.88 to 2.15 Å. The Sr²⁺ and La³⁺/Yb³⁺ cations randomly occupy the same 4e site with IX-fold O²⁻ coordination (1×O2, 4×O1 and 4×O2) forming a mono-capped tetragonal anti-prismatic geometry. The metal (M = Sr|La|Yb) – oxygen interatomic distances for the [MO₉] polyhedra are 2.38–2.68 Å. The anions (O²⁻) are distributed over the 4c (O1) and 4e (O2) sites. The crystal structure of Yb:SLA is determined by a condensed framework of corner-sharing [AlO₆] and [MO₉] polyhedra forming a “cage” structure, Fig. 3a. These polyhedra form infinite layers parallel to the a - b plane, Fig. 3b.

Experimental

The tetragonal Yb:SLA has two principal thermal expansion coefficients, α_a and α_c (along the a - and c -axes, respectively). To measure them, a thermal mechanical analyzer (Diamond TMA, Perkin Elmer) was used. The sample was processed as a rectangular piece with dimensions $5.37(a) \times 6.25(b) \times 4.57(c)$ mm³.

The specific heat C_p was measured by differential scanning calorimetry (DSC) using a simultaneous thermal analyzer (Diamond DSC, Perkin Elmer).

The thermal diffusivities D_a and D_c were measured using a laser flash apparatus (LFA457, NETZSCH). Two square wafers from Yb:SLA were used for the measurements with dimensions $6.0(a) \times 6.0(b) \times 2.0(c)$ mm³ and $6.0(c) \times 6.0(b) \times 2.0(a)$ mm³. They were coated with graphite on both 6×6 mm² sides.

Yb:SLA is an optically uniaxial crystal. Its optical axis is parallel to the crystallographic c -axis. Thus, there are two

principal light polarizations, π ($\mathbf{E} \parallel \mathbf{c}$) and σ ($\mathbf{E} \perp \mathbf{c}$). One polished sample with dimensions of $3.0(\mathbf{c}) \times 5.0(\mathbf{a}) \times 7.0(\mathbf{b})$ mm³ was cut from the as-grown crystal for polarized spectral measurements.

The polarized absorption spectra at RT were measured with a Varian CARY-5000 spectrophotometer. For low-temperature (LT, 6 K) studies, an Oxford Instruments Ltd. cryostat (model SU 12) with helium-gas close-cycle flow was used. The spectra were measured with polarized light (π and σ) using a Glan-Taylor polarizer. The spectral resolution was 0.1 nm.

The polarized luminescence spectra at RT were measured with a YOKOGAWA optical spectrum analyzer (OSA), model AQ 6373. For LT studies, the same cryostat was used.

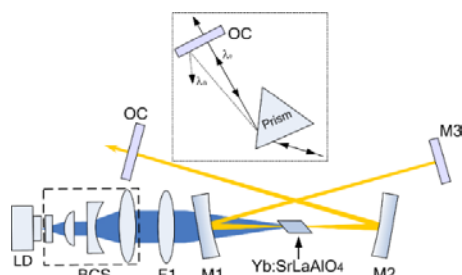


Fig. 4 Scheme of the diode-pumped tunable CW Yb:SLA laser. BCS: Beam collimating system; F1: Focus lens; M1 and M2: Folding mirrors; M3: plane mirror; OC: Output coupler.

The Glan-Taylor polarizer enabled polarization-resolved studies. The spectral resolution was 0.1 nm. An InGaAs laser diode emitting at ~ 973 nm was used as an excitation source.

The luminescence decay curve was measured at RT at a wavelength of 1020 nm using a mechanically modulated pump beam from the InGaAs diode, OSA and a 2 GHz Tektronix DPO5204B digital oscilloscope.

The polarized Raman spectra were measured with a Renishaw inVia confocal micro-Raman microscope with a x50 objective and a 1800 gr/mm grating. The excitation wavelength λ_{exc} was 514 nm (Ar⁺ ion laser). The spectral resolution was 1 cm⁻¹.

The laser tuning experiments were performed in a X-folded cavity, Fig. 4. More details can be found in Ref. [6]. The c -cut sample had a length of 3.0 mm and a cross section of 3.0×3.0 mm². It was placed at a Brewster angle between two folding concave mirrors M₁ and M₂ (radius of curvature, RoC = -100 mm). The crystal was wrapped with In foil and tightly mounted in a water-cooled Cu-block. The pump source was a two-section distributed Bragg-reflector tapered InGaAs diode-laser (DBR-TDL) with a maximum output power of 6 W at 980 nm. The pump light was focused to a spot with a diameter of 35 μ m in the crystal using a homemade beam collimating system and a spherical focusing lens (F1) with a focal length of 100 mm. The crystal was pumped through the M₁ mirror serving as a pump mirror. The pumping was in a single-pass and the pump absorption amounted to $\sim 30\%$. A prism was inserted into the cavity as a wavelength tuning element, close to the output coupler (OC).

Results and discussion

Thermal properties

The knowledge of the thermal properties of a crystal is relevant both for the crystal growth and its laser applications.

The measured thermal expansion curves of the Yb:SLA crystal (relative sample elongation, $\Delta L/L_0$, vs. the temperature) are shown in Fig. 5a. These dependences are almost linear for the directions along the a - and c -axes over the studied temperature range of 300–775 K.

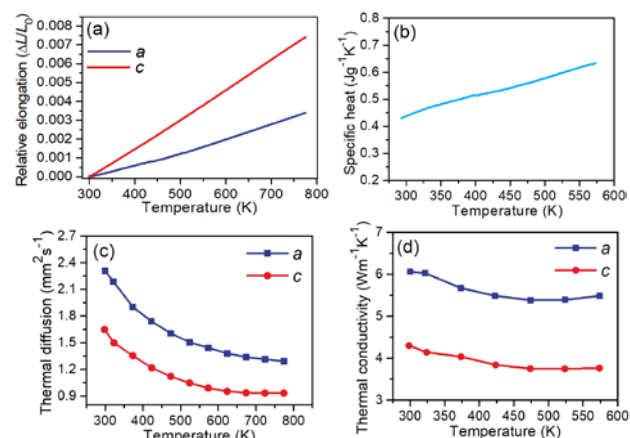


Fig. 5 (a-d) Thermal and thermo-mechanical characteristics of Yb:SLA: (a) thermal expansion measurement; (b) measured specific heat C_p ; (c) measured thermal diffusivity D ; (d) calculated thermal conductivity κ .

According to Fig. 5a, the mean values of the linear thermal expansion coefficients along the a - and c -axes were calculated to be $a_a = 7.23$ and $a_c = 15.75$ [10^{-6} K^{-1}]. This indicates a relatively strong anisotropy (ratio $a_c/a_a = 2.2$). Therefore, to protect the Yb:SLA crystal from possible cracking caused by the anisotropic thermal expansion, a smaller and stepped cooling rate should be used during the crystal growth.

The measured dependence of the specific heat of Yb:SLA on temperature is shown in Fig. 5b. The C_p value varies almost linearly, increasing from 0.43 to $0.63 \text{ Jg}^{-1}\text{K}^{-1}$ when the temperature is elevated from 293 to 573 K. The specific heat of Yb:SLA is $0.44 \text{ Jg}^{-1}\text{K}^{-1}$ at 300 K. In comparison with Yb:YAG ($C_p = 0.60 \text{ Jg}^{-1}\text{K}^{-1}$), Yb:CaYAlO₄ ($C_p = 0.59 \text{ Jg}^{-1}\text{K}^{-1}$) and Yb:CaGdAlO₄ ($C_p = 0.45 \text{ Jg}^{-1}\text{K}^{-1}$) at 300 K [18–20], this value is closer to that of Yb:CaGdAlO₄.

Figure 5c shows the measured thermal diffusivities of the Yb:SLA crystal. Both values measured along the a - and c -axes decrease with increasing temperature. At 300 K, they are $D_a = 2.307$ and $D_c = 1.648 \text{ mm}^2\text{s}^{-1}$.

Figure 5d shows the calculated temperature dependence of the thermal conductivity of Yb:SLA along the a - and c -axes, calculated using the formula $\kappa_i = D_i \times \rho \times C_p$, here $i = a, c$ and $\rho = 5.92 \text{ g/cm}^3$ is the measured crystal density (at RT). Both κ_a and κ_c values decrease with increasing temperature and for temperatures higher than 474 K, this dependence is almost saturated. At 300 K, the thermal conductivities along the a - and c -axes are 6.06 and $4.30 \text{ Wm}^{-1}\text{K}^{-1}$, respectively.

Table 3. Comparison of basic properties of Yb:SLA with several disordered crystals.

Crystals	Yb:SLA	Yb:Ca ₄ YO(BO ₃) ₃	Yb:NaY(WO ₄) ₂	Yb:CaYAIO ₄	Yb:CaGdAlO ₄
Crystal system	tetragonal	monoclinic	tetragonal	tetragonal	tetragonal
Growth method	Cz	Cz	Cz	Cz	Cz
κ (Wm ⁻¹ K ⁻¹)	6.1(a), 4.3(c) (1.36 at.%)	~2.1	1.1(a), 1.2(c)	3.6(a), 3.2(c) (1.0 at.%)	6.9(a), 6.3(c) (1.2 at.%) 5.3(a), 4.4(c) (undoped)
FWHM at λ_{abs} (nm)	24 (π), 13 (σ)	2.3-4	55 (π), 45 (σ)	12 (π), 13 (σ)	17 (π), 29 (σ)
σ_{abs} (10 ⁻²⁰ cm ²)	2.58 (π), 1.45 (σ)	1.05	1.70 (π), 1.12 (σ)	5.68 (π), 1.97 (σ)	2.65 (π), 1.03 (σ)
FWHM at λ_{lum} (nm)	89 (σ)	44-45	40	76 (σ)	77 (σ)
σ_{SE} (10 ⁻²⁰ cm ²)	0.80 (plateau, σ)	0.1-0.45	0.92-0.14	0.80 (plateau, σ)	0.75 (plateau, σ)
Fluorescence lifetime (ms)	0.63 (meas.), 0.55 (est.)	2.3	0.51	0.43	0.42 (meas.), 0.39 (est.)
ML pulse duration (fs)	-	35	45	30	32
Reference	This work	[5,21-23]	[7,24-26]	[8,19]	[9,16,20,27]

(a) and (c) - along the **a** and **c** crystallographic axes; (π) and (σ) indicate the light polarization

In Table 3, laser relevant parameters of Yb:SLA are compared with other Yb-doped disordered crystals. All of the latter excel the generation of sub-50 fs pulses in ML lasers. The thermal conductivity of Yb:SLA is higher than that of Yb:Ca₄YO(BO₃)₃, Yb:NaY(WO₄)₂ and Yb:CaYAIO₄, and almost as high as that of Yb:CaGdAlO₄. This feature makes Yb:SLA to be very suitable also for high-power laser performance.

Optical spectroscopy

To determine the Stark splitting of the ground state (²F_{7/2}, sub-levels 0...3) and the excited-state (²F_{5/2}, sub-levels 0'...2') of Yb³⁺ ions in SLA, we have measured the low-temperature (6 K) absorption and emission spectra for two principal light polarizations (π and σ) using an **a**-cut Yb:SLA crystal. The measured spectra are shown in Fig. 6. Their assignment was performed following Ref. [28] for an isostructural CaYAIO₄ crystal and the Raman spectra of Yb:SLA (see below) in order to exclude the vibronic (phonon-assisted) transitions. At 6 K, the absorption spectrum contains an intense peak at 982.0 nm (10193 cm⁻¹) corresponding to the transition between the lowest Stark sub-levels of two multiplets, 0 → 0' (zero-phonon line, ZPL). It is very broad (the full width at half maximum, FWHM, is about 2 nm) even at 6 K. The emission spectra contain multiple lines at >1000 nm due to the 0' → 1...3 transitions and the emission band extends until at least 1.12 μm even at 6 K.

According to the assignment of the electronic transitions, we plotted the scheme of energy levels of Yb³⁺ ions in SLA, see Fig. 7. The total splitting of the ground-state is 606 cm⁻¹ which is favorable for a wavelength tunable laser operation. In Fig. 7, we also indicate the calculated partition functions $Z_{1(2)}$. The ratio $Z_1/Z_2 = 1.16$. This value is close to those reported recently for Yb³⁺-doped CaLnAlO₄ crystals [29].

To derive the optimum pumping conditions of Yb:SLA lasers and to determine the absorption, σ_{abs} , and stimulated-emission (SE), σ_{SE} , cross-sections of Yb³⁺ ions, the polarized absorption and luminescence measurements were performed at RT. The σ_{SE} spectra were calculated by a combination of

Füchtbauer–Ladenburg (F-L) formula and reciprocity method (RM) [30,31]:

$$\sigma_{\text{SE}}^i(\lambda) = \frac{1}{8\pi n^2 c \tau_{\text{rad}}} \frac{\lambda^5 W_i(\lambda)}{1/3 \sum_{i=\sigma,\pi} \int \lambda W_i(\lambda) d\lambda}, \quad (1)$$

$$\sigma_{\text{SE}}^i(\lambda) = \sigma_{\text{abs}}^i(\lambda) \frac{Z_1}{Z_2} \exp\left(-\frac{hc/\lambda - E_{\text{ZPL}}}{kT}\right), \quad (2)$$

where $i = \pi$ or σ , c is the speed of light, h is the Planck constant, k is the Boltzmann constant, T is the temperature ($T = \text{RT}$), λ is the light wavelength, $W_i(\lambda)$ is the measured emission spectrum for i -th polarization, n is the refractive index (an approximate value of 1.90 was taken [32]) and τ_{rad} is the radiative lifetime of the emitting state (²F_{5/2}) which was estimated to be 0.55 ms by using the modified reciprocity method.

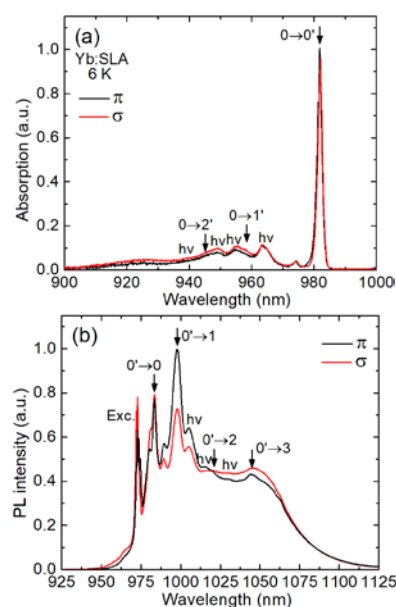


Fig. 6 Low-temperature (6 K) spectroscopy of the Yb:SLA crystal: (a) absorption and (b) luminescence spectra for light polarizations π and σ ($\lambda_{\text{exc}} = 973$ nm). Arrows indicate the transitions between the Stark sub-levels, $h\nu$ stands for the vibronic bands.

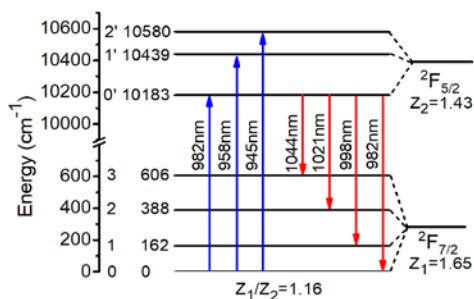


Fig. 7 Scheme of the Stark splitting of the Yb^{3+} multiplets in the SLA crystal: *Arrows* indicate the transitions accounting for absorption and emission, $Z_{1(2)}$ are the partition functions.

Figure 8 shows the absorption and SE cross-sections for the ${}^2\text{F}_{7/2} \leftrightarrow {}^2\text{F}_{5/2}$ transition of Yb^{3+} in SLA and the two polarization directions (π and σ) at RT. Both the absorption and emission spectra show a notable polarization anisotropy.

The maximum σ_{abs} amounts to $2.58 \times 10^{-20} \text{ cm}^2$ at 980.2 nm (ZPL) with a FWHM of the absorption peak of 24 nm (for π polarization). For σ polarization, the maximum σ_{abs} value is 1.8 times lower and the absorption peak is narrower, FWHM = 14 nm. The values of σ_{abs} for Yb:SLA are comparable to those for the well-known disordered crystals (see Table 3), and 4 times larger than that of Yb:YAG [33]. The broad ZPL absorption peak in Yb:SLA at 980 nm partially results from the disordered crystal structure and makes it very suitable for pumping with InGaAs laser diodes.

The maximum σ_{SE} value for Yb:SLA is $2.88 \times 10^{-20} \text{ cm}^2$ at 980.2 nm (for π polarization). In the spectral range where laser operation is expected, the σ polarization shows higher SE cross-sections. The σ_{SE} spectrum contains a flat, smooth, and relatively intense ($\sim 0.6 \times 10^{-20} \text{ cm}^2$) plateau that extends from 1010 to 1060 nm. Moreover, for this polarization, the measured emission spectrum has a considerably large FWHM of 89 nm, which is broader than those for all crystals listed in Table 3. This spectral feature is particularly suitable for the generation of a broad laser spectrum. Thus, the generation of ultrashort pulses are expected with this Yb^{3+} -doped crystal.

In the quasi-three-level laser system of Yb^{3+} , the potential gain bandwidth for tunable or ML operation can be estimated by calculating the gain cross-section according to $\sigma_{\text{gain}} = \beta\sigma_{\text{SE}} - (1 - \beta)\sigma_{\text{abs}}$, where β denotes the ratio of the inverted ions to the total Yb^{3+} -ion density. The gain cross-sections are shown in Fig. 9 for the two polarizations σ and π . From these curves, it can be expected that, for a constant β , the oscillation

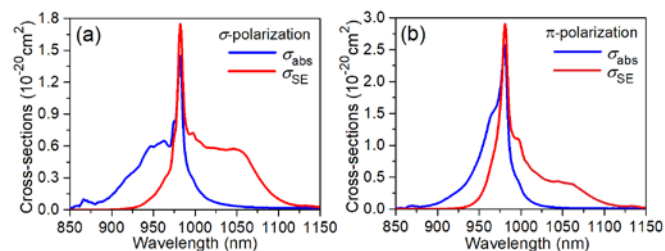


Fig. 8 RT absorption, σ_{abs} , and stimulated-emission, σ_{SE} , cross-sections of Yb:SLA for light polarizations (a) σ and (b) π . The σ_{SE} spectra are determined by a combination of Eqs. (1)-(2).

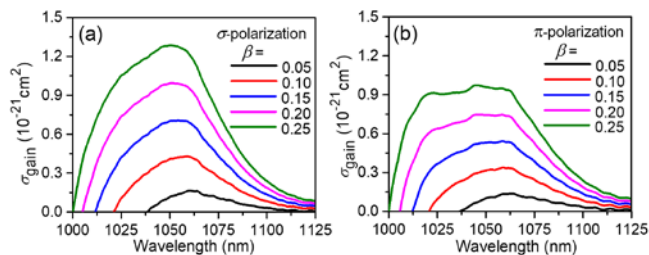


Fig. 9 RT gain cross-sections, $\sigma_{\text{gain}} = \beta\sigma_{\text{SE}} - (1 - \beta)\sigma_{\text{abs}}$, for Yb:SLA, for the σ and π polarizations and different population inversion rates $\beta = N_2({}^2\text{F}_{5/2})/N_{\text{Yb}}$.

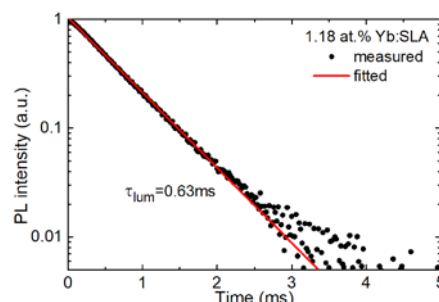


Fig. 10 RT luminescence decay curve of the ${}^2\text{F}_{5/2}$ manifold of Yb:SLA: *symbols* – experimental data, *red line* – single-exponential fit.

wavelength will be slightly shorter and the gain will be larger for the σ polarization. Apparently, the results also show that the Yb:SLA has broad and remarkably flat gain spectra for both polarizations.

The fluorescence decay curve of a 1.18 at.% Yb:SLA crystal is shown in Fig. 10. By a single-exponential fitting, the fluorescence lifetime τ_{lum} was found to be 0.63 ms, which is slightly longer than the estimated τ_{rad} due to the reabsorption effect.

Raman spectroscopy

The vibronic properties of Yb:LSA were studied using Raman spectroscopy. The polarized Raman spectra for *a*-cut and *c*-cut crystals and π and σ light polarizations are shown in Fig. 11. The spectra are strongly polarized. The factor group analysis of the D^{17}_{4h} unit cell predicts the following irreducible representations at the center of the Brillouin zone ($k = 0$): $\Gamma = 2A_{1g} + 2E_g + 4A_{2u} + 5E_u + B_{2u}$. The $2A_{1g}$ and $2E_g$ modes are Raman active, $3A_{2u}$ and $4E_u$ are IR active, $1A_{2u}$ and $1E_u$ are acoustic whereas B_{2u} is silent [34]. In Fig. 11,

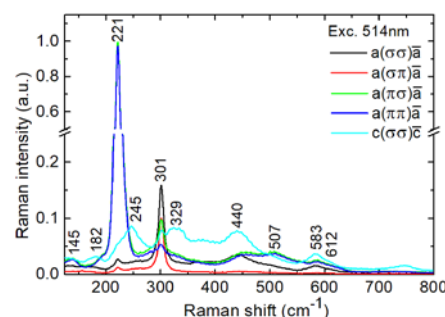


Fig. 11 Polarized Raman spectra for the Yb:SLA crystal, $\lambda_{\text{exc}} = 514 \text{ nm}$. *Numbers* denote the Raman peak frequencies in cm^{-1} .

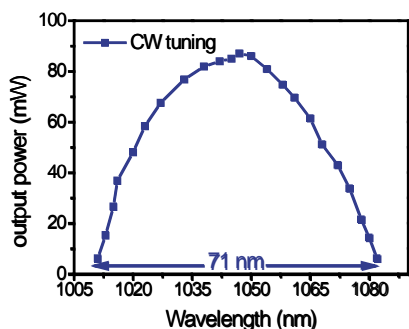


Fig. 12 Wavelength tuning curve of a diode-pumped CW Yb:SLA laser, $T_{oc} = 0.5\%$, the laser set-up is depicted in Fig. 4. The laser polarization is σ .

only four bands correspond to the Raman-active modes, namely, the most intense band at 221 cm^{-1} (A_{1g}) related to the Sr/La vibrations along the c -axis, the second intense band at 301 cm^{-1} (E_g) related to the O vibrations in the a - b plane, and two weak bands at 145 cm^{-1} (E_g) and 507 cm^{-1} (A_{1g}).

Thus, LSA is a low-phonon-energy material which is favorable for weak non-radiative relaxation. In addition to the above mentioned four modes, additional weak bands (especially for the c -cut crystal) are resolved at 182, 245, 329, 440, 583 and 612 cm^{-1} . They can be partially assigned to second-order scattering and defect-induced modes.

Laser tuning performance

Figure 12 shows the laser tuning performance of Yb:SLA obtained for OC with a transmission of 0.5% at the laser wavelength. The laser was continuously tuned from 1011 to 1082 nm (tuning range: 71 nm at zero-level).

The tuning curve is very smooth and symmetric. The maximum of the laser output is observed around 1050 nm in agreement with the gain spectra for σ -polarization, Fig. 9a. Previously, tuning of laser emission with Yb:CaGdAlO₄ and Yb:CaYAlO₄ crystals was demonstrated, leading to tuning ranges of 91 nm (for 0.4% OC) and 55 nm (for 5% OC), respectively [17,35].

Conclusions

A large volume and high optical quality tetragonal Yb:SrLaAlO₄ (Yb:SLA) aluminate laser crystal has been grown by the Czochralski method. Its thermal, spectroscopic and tuning laser performance were investigated. The thermal conductivities of Yb:SLA at RT are 6.06 and $3.75\text{ Wm}^{-1}\text{K}^{-1}$ along the a and c axes, respectively. Such high values and the expected positive thermal lens being characteristic for ABCO₄-type crystals [36] and promotes Yb:LSA crystals for power-scalable lasers at $\sim 1\text{ }\mu\text{m}$. Absorption, stimulated-emission and gain cross-sections of Yb:SLA are derived. For π -polarization, the maximum σ_{abs} is $2.58 \times 10^{-20}\text{ cm}^2$ at 980.1 nm corresponding to a FWHM of 24 nm. The maximum σ_{SE} in the spectral range where laser operation is expected amounts to $0.57 \times 10^{-20}\text{ cm}^2$ at $\sim 1050\text{ nm}$, for σ polarization and the emission bandwidth is 89 nm. Broad and flat gain spectra for both polarizations (π and σ) are calculated. A

broad wavelength tuning range of 71 nm has been achieved in a diode-pumped c -cut Yb:SLA laser. All of these results show that the Yb:SLA crystal exhibits attractive thermal properties together with smooth and broad emission bands, which make it promising for ultrashort pulse generation and high-power lasers.

Conflicts of interest

There are no conflicts to declare.

Acknowledgements

The research is partially supported by the National Natural Science Foundation of China (No. 51402268); the Institute of Chemical Materials, China Academy of Engineering Physics (Grant No.32203); China Scholarship Council (CSC). This work was supported by the Spanish Government under projects MAT2016-75716-C2-1-R (AEI/FEDER,UE) and TEC2014-55948-R, and by the Generalitat de Catalunya under project 2017SGR755. F.D. acknowledges additional support through the ICREA academia award 2010ICREA-02 for excellence in research. P.L. acknowledges financial support from the Government of the Russian Federation (Grant 074-U01) through ITMO Post-Doctoral Fellowship scheme.

References

- 1 C. Hönninger, R. Paschotta, M. Graf, F. Morier-Genoud, G. Zhang, M. Moser, S. Biswal, J. Nees, A. Braun, G. A. Mourou and I. Johannsen, *Appl. Phys. B*, 1999, **69**, 3-17.
- 2 W.F. Krupke, *IEEE J. Sel. Top. Quantum Electron.*, 2000, **6**, 1287-1296.
- 3 P.O. Petit, J. Petit, P. Goldner and B. Viana, *Opt. Mater.*, 2008, **30**, 1093-1097.
- 4 A. García-Cortés, C. Zaldo and C. Cascales, *Opt. Mater.*, 2009, **31**, 1096-1100.
- 5 A. Yoshida, A. Schmidt, V. Petrov, C. Fiebig, G. Erbert, J. Liu, H. Zhang, J. Wang and U. Griebner, *Opt. Lett.*, 2011, **36**, 4425-4427.
- 6 J. Ma, Z. B. Pan, J. Wang, H. L. Yuan, H. Q. Cai, G. Q. Xie, L. J. Qian, D. Y. Shen and D. Y. Tang, *Opt. Express*, 2017, **25**, 14968-14973.
- 7 J. Ma, H. Huang, H. Yu, H. Zhang and D. Tang, *IEEE Photon. Technol. Lett.*, 2016, **28**, 1298-1301.
- 8 J. Ma, H. Huang, K. Ning, X. Xu, G. Xie, L. Qian, K. P. Loh and D. Tang, *Opt. Lett.*, 2016, **41**, 890-893.
- 9 P. Seviliano, P. Georges, F. Druon, D. Descamps and E. Cormier, *Opt. Lett.*, 2014, **39**, 6001-6004.
- 10 S. D. Liu, L. L. Dong, X. Zhang, Y. P. Yao, Y. Xu, T. Q. Ren, L. H. Zheng, L. B. Su and M. Berkowski, *Opt. Mater.*, 2017, **64**, 351-355.
- 11 S. D. Liu, L. L. Dong, L. H. Zheng, M. Berkowski, L. B. Su, T. Q. Ren, Y. D. Peng, J. Hou, B. T. Zhang and J. L. He, *Appl. Phys. Express*, 2016, **9**, 072701.
- 12 R. Brown, V. Pendrick, D. Kalokitis and B. H. T. Chai, *Appl. Phys. Lett.*, 1990, **57**, 1351-1353.
- 13 A. Pajaczowska, A. Gloubokov, A. Klos and C. F. Woensdregt, *J. Cryst. Growth*, 1997, **171**, 387-391.

- 14 A. Gloubokov, R. Jablonski, W. Ryba-Romanowski, J. Sass, A. Pajaczkowska, R. Uecker and P. Reiche, *J. Cryst. Growth*, 1995, **147**, 123-129.
- 15 D. Klimm, P. Reiche, R. Uecker and S. Ganschow, *Cryst. Growth Des.*, 2001, **1**, 321-325.
- 16 J. Q. Di, X. D. Xu, C. T. Xia, L. H. Zheng, G. Aka, H. H. Yu, Q. L. Sai, X. Y. Guo and L. Zhu, *Laser Phys.*, 2016, **26**, 045803.
- 17 K. Beil, B. Deppe and C. Kränkel, *Opt. Lett.*, 2013, **38**, 1966-1968.
- 18 R. L. Aggarwal, D. J. Ripin, J. R. Ochoa and T. Y. Fan, *J. Appl. Phys.*, 2005, **98**, 103514.
- 19 D. Z. Li, X. D. Xu, H. M. Zhu, X. Y. Chen, W. D. Tan, J. Zhang, D. Y. Tang, J. Ma, F. Wu, C. T. Xia and J. Xu, *J. Opt. Soc. Am. B*, 2011, **28**, 1650-1654.
- 20 Q. Q. Hu, Z. T. Jia, C. Tang, N. Lin, J. Zhang, N. Jia, S. P. Wang, X. Zhao and X. T. Tao, *CrystEngComm*, 2017, **19**, 537-545.
- 21 H. Zhang, X. Meng, P. Wang, L. Liu, R. Cheng, J. Dawes, P. Dekker, S. Zhang and L. Sun, *Appl. Phys. B*, 1999, **68**, 1147-1149.
- 22 A. Aron, G. Aka, B. Viana, A. Kahn-Harari, D. Vivien, F. Druon, F. Balembois, P. Georges, A. Brun, N. Lenain and M. Jacquet, *Opt. Mater.*, 2001, **16**, 181-188.
- 23 T. Südmeyer, C. Kränkel, C. R. E. Baer, O. H. Heckl, C. J. Saraceno, M. Golling, R. Peters, K. Petermann, G. Huber and U. Keller, *Appl. Phys. B*, 2009, **97**, 281-295.
- 24 J. D. Fan, H. J. Zhang, J. Y. Wang, Z. C. Ling, H. R. Xia, X. F. Chen, Y. G. Yu, Q. M. Lu and M. H. Jiang, *J. Phys. D: Appl. Phys.*, 2006, **39**, 1034-1041.
- 25 J. H. Feng, J. L. Xu, Z. J. Zhu, Y. Wang, Z. Y. You, J. F. Li, H. Y. Wang and C. Y. Tu, *J. Alloy Compd.*, 2013, **566**, 229-234.
- 26 Y. Cheng, X. D. Xu, X. B. Yang, Z. Xin, D. H. Cao and J. Xu, *Laser Phys.*, 2009, **19**, 2133-2139.
- 27 Y. Zaouter, J. Didierjean, F. Balembois, G. Lucas Leclin, F. Druon and P. Georges, *Opt. Lett.*, 2006, **31**, 119-121.
- 28 J. A. Hutchinson, H. R. Verdun, B. H. Chai, B. Zandi and L. D. Merkle, *Opt. Mater.*, 1994, **3**, 287-306.
- 29 P. Loiko, J. M. Serres, X. Mateos, X. Xu, J. Xu, V. Jambunathan, P. Navratil, A. Lucianetti, T. Mocek, X. Zhang, U. Griebner, V. Petrov, M. Aguiló, F. Díaz and A. Major, *Opt. Lett.*, 2017, **42**, 2431-2434.
- 30 B. F. Aull and H. P. Janssen, *IEEE J. Quantum Electron.*, 1982, **18**, 925-930.
- 31 S. A. Payne, L. L. Chase, L. K. Smith, W. L. Kway and W. F. Krupke, *IEEE J. Quantum Electron.*, 1992, **28**, 2619-2630.
- 32 O. Medenbach and R. D. Shannon, *J. Opt. Soc. Am. B*, 1997, **14**, 3299-3318.
- 33 L. D. DeLoach, S.A. Payne, L. L. Chase, L. K. Smith, W. L. Kway and W.F. Krupke, *IEEE J. Quantum Electron.*, 1993, **29**, 1179-1191.
- 34 V. G. Hadjiev, M. Cardona, I. Ivanov, V. Popov, M. Gyulmezov, M. N. Iliev and M. Berkowski, *J. Alloy Compd.*, 1997, **251**, 7-10.
- 35 W.D. Tan, D.Y. Tang, X.D. Xu, D.Z. Li, J. Zhang, C.W. Xu, Z.H. Cong and J. Xu, *Laser Phys. Lett.*, 2011, **8**, 193-196.
- 36 P. Loiko, F. Druon, P. Georges, B. Viana and K. Yumashev, *Opt. Mater. Express*, 2014, **4**, 2241-2249.